

Damped Dreamlet Representation for Exploration Seismic Data Interpolation and Denoising

Weilin Huang^{ID}, Ru-Shan Wu, and Runqiu Wang

Abstract—The dreamlet (drumbeat-beamlet) transform can provide us an efficient method to represent physical wavefield, because the dreamlet basis satisfies automatically the wave equation, which is a distinctive feature different from mathematical basis, such as Fourier and curvelet. It can obtain an estimation of true signal from the observed noisy data by abandoning those insignificant components in the dreamlet domain. However, we have found that a more accurate estimation can be achieved by a damped version of the dreamlet representation. We have theoretically derived the damped dreamlet representation and given its geometric interpretation and analysis. Two applications of the proposed method have been explored in this paper: seismic random noise suppression and seismic data interpolation. Various examples demonstrate that the damped dreamlet representation-based technique has a superior performance compared with the mathematical-basis-based representation and rank-reduction-based techniques.

Index Terms—Damping operator, dreamlet, physical wavelet, seismic data interpolation, seismic random noise suppression, sparse representation.

I. INTRODUCTION

REAL-world signals are always contaminated by various types of noise. The estimation of true signals from the observed noisy data is an important procedure in varieties of signal-analysis applications across different scientific domains. In seismic exploration, a high signal-to-noise ratio (SNR) is desirable for various procedures, such as amplitude variation with offset analysis, seismic attribute analysis, and microseismic monitoring. The suppression of incoherent noise is a tough issue [1], [2]. Over the past few decades, researchers put a lot of effort into separating signal and incoherent noise and developed abundant approaches coming from various fields, such as median filtering [3], prediction filtering [4], empirical mode decomposition [5]–[7],

Manuscript received August 24, 2017; revised November 15, 2017 and January 10, 2018; accepted January 11, 2018. This work was supported in part by the National Science and Technology Major Project under Grant 2016ZX05023004 and in part by the WTOPI Research Consortium at University of California at Santa Cruz, Santa Cruz, CA, USA. The work of W. Huang was supported by the China Scholarship Council. (*Corresponding author: Weilin Huang*.)

W. Huang is with the State Key Laboratory of Petroleum Resources and Prospecting, China University of Petroleum, Beijing 102249, China, and also with the Modeling and Imaging Laboratory, University of California at Santa Cruz, Santa Cruz, CA 95064 USA (e-mail: cup_hwl@126.com).

R. S. Wu is with the Modeling and Imaging Laboratory, University of California at Santa Cruz, Santa Cruz, CA 95064 USA.

R. Wang is with the State Key Laboratory of Petroleum Resources and Prospecting, China University of Petroleum, Beijing 102249, China.

Color versions of one or more of the figures in this paper are available online at <http://ieeexplore.ieee.org>.

Digital Object Identifier 10.1109/TGRS.2018.2793856

time–frequency peak filtering [8]–[10], rank-reduction [2], [11]–[14], mathematical morphological filtering [15]–[17], various mathematical transforms [18]–[20], [20]–[22], dictionary learning [23]–[25], multitask [26]–[28], and inversion-based approaches [29]–[35]. Due to the presence of obstacles, forbidden areas, and feathering in the seismic exploration area, the seismic data acquisition usually does not have regular sampling. However, almost all the existing seismic processing techniques are based on the assumption and precondition of regularly sampled input data. Seismic interpolation is such a preprocessing step to provide the regularly sampled seismic data. It is also a cheap way to obtain high-capacity data for high-resolution imaging and inversion. The techniques of seismic data interpolation can be divided into several categories. The first category is the prediction-based approaches, in which a prediction error filter is designed such that the predicted data and the existing data have the minimum misfit by solving a least-squares linear inverse problem [36]–[38]. The second category treats the seismic data reconstruction as a low-rank tensor or a matrix completion problem [39]. This category of approaches exploits the fact that the irregular data decimation and incoherent noise will increase the rank of a data matrix or a tensor. Examples are the singular spectrum analysis (SSA) method (or Cadzow filtering) [40]–[42] and the matrix factorization approach [39], [43], [44].

Recently, compressed sensing-based seismic reconstruction techniques [45] become popular and attract the attentions of a lot of researchers. The central idea of this category of approaches is that it assumes that the signal is compressible in a certain transformed domain but the incoherent noise and irregular data decimation are not. With the help of certain sparsity-promoting transform, the energy of signal is compressed in the subspace corresponding to some greater coefficients. Thus, we can obtain an estimation of signal by abandoning those nonsignificant coefficients (set them to zero). Various sparsity-promoting transforms have been studied for the compressed sensing-based seismic reconstruction, for example, the Fourier transform [46], [47], the wavelet transform [21], the curvelet transform [48], the Radon transform [49], [50], and the seislet transform [51], [52]. A physical wavelet was formally introduced by Kaiser [53], as the localized wave solution to the wave equation by extending the solution to the complex space–time [54]. The physical wavelet packet naturally satisfies the wave equation and therefore has a more efficient representation of the physical wavefield (e.g., seismic data) compared with the aforementioned mathematical-basis representations [54], [55]. The dreamlet

(drumbeat-beamlet), as a type of physical wavelet, was first introduced by Wu *et al.* [55]. It is defined as a tensor product of time–frequency domain drumbeat and space–wavenumber beamlet [56]. The dreamlet has a decent ability in the representation of the seismic data, because it is localized on the light cone in the 4-D Fourier space, which is a feasible region of the wave solutions. For this reason, the dreamlet representation can be an efficient method to estimate the true signal from the observed noisy seismic data because of the high sparsity of the seismic signals in the dreamlet domain [57], [58]. However, our recent study shows that a more accurate estimation can be achieved by a damped version of the dreamlet representation. We have found that the conventional dreamlet representation is to find a projection of the observed data from a whole space (i.e., the observed data-dimensional space) onto a subspace (i.e., the signal-dimensional subspace) under the dreamlet basis. As the true signal is unequal to this projection, there is a gap between them. The damped dreamlet representation is designed to narrow the gap. This process can be conceptually understood as a kind of the double least-squares projections [59]. In order to test the proposed method, we apply it to two problems of exploration seismic processing, namely, the seismic random noise suppression and seismic data interpolation. The outstanding performance of the proposed approach is demonstrated from the two applications.

II. THEORY

A. Dreamlet Representation

As a type of physical wavelet, the dreamlet (drumbeat-beamlet) is defined on an observation plane. The observation plane could be the earth surface or a subsurface at depth z during wavefield extrapolation [55]. A dreamlet atom is defined as the tensor product of drumbeat atom (time–frequency atom) and beamlet atom (space–wavenumber atom) in decomposing the wavefield on an observation plane which obeys the causal relation or the dispersion relation [54], [60]. A dreamlet atom can be formulated as the following form [57], [58]:

$$d_{\bar{t}\bar{\omega}\bar{x}\bar{\xi}}(t, x) = g_{\bar{t}\bar{\omega}}(t)b_{\bar{x}\bar{\xi}}(x) \quad (1)$$

where

$$g_{\bar{t}\bar{\omega}}(t) = W(t - \bar{t})e^{-i\bar{\omega}t} \quad (2)$$

is the time–frequency atom: “drumbeat” with $W(t)$ as a smooth window function and

$$b_{\bar{x}\bar{\xi}}(x) = B(x - \bar{x})e^{i\bar{\xi}x} \quad (3)$$

is the space–wavenumber atom: “beamlet” with $B(t)$ as a bell function [56]. x and t are space and time indices, respectively. The bars over letters signify that the variables are local variables related to the window centers, i.e., \bar{t} , $\bar{\omega}$, \bar{x} , and $\bar{\xi}$ denote the local time, local frequency, local space, and local wavenumber, respectively. By substituting (2) and (3) into (1), we hold a localized wave-packet (the dreamlet packet) in time–space plane

$$d_{\bar{t}\bar{\omega}\bar{x}\bar{\xi}}(t, x) = W(t - \bar{t})B(x - \bar{x})e^{-i(\bar{\omega}t - \bar{\xi}x)}. \quad (4)$$

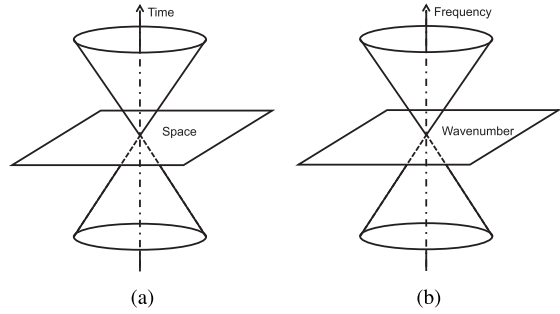


Fig. 1. Demonstration of the light cones. (a) Causality hypersurface in the space–time domain. (b) Dispersion hypersurface in the frequency–wavenumber domain.

Accordingly, the seismic data $\mathbf{U} = [u(t, x)]$ can be represented by the dreamlet packet as

$$u(t, x) = \sum_{\bar{t}\bar{\omega}\bar{x}\bar{\xi}} [c_{\bar{t}\bar{\omega}\bar{x}\bar{\xi}} d_{\bar{t}\bar{\omega}\bar{x}\bar{\xi}}(x, t)] \quad (5)$$

where

$$c_{\bar{t}\bar{\omega}\bar{x}\bar{\xi}} = \int \int u(t, x) \hat{d}_{\bar{t}\bar{\omega}\bar{x}\bar{\xi}}^*(t, x) dt dx \quad (6)$$

is the coefficient. Symbol $*$ denotes the complex conjugate. $\hat{d}_{\bar{t}\bar{\omega}\bar{x}\bar{\xi}}(t, x)$ is the unitary dual frame of $d_{\bar{t}\bar{\omega}\bar{x}\bar{\xi}}(t, x)$ satisfying

$$1 = \int \int \hat{d}_{\bar{t}\bar{\omega}\bar{x}\bar{\xi}}(t, x) d_{\bar{t}\bar{\omega}\bar{x}\bar{\xi}}(t, x) dt dx. \quad (7)$$

B. Comparison Between Dreamlet and Mathematical Atoms

The most significant difference between the dreamlet base (atom) and mathematical basis (atoms) (e.g., Fourier, ridgelet, and curvelet basis) is that the dreamlet atom is constructed in the way that it not only possess the properties of the wavelet but also satisfies wave equation automatically and, therefore, can represent the seismic data effectively [54]. Note that the phase terms in the time–frequency atom (2) and the space–wavenumber atom (3) have opposite signs. This is consistent with the causality relation imposed by the wave equation. Under the physical rules of seismic wave propagation, the time–space distributions of seismic signals recorded on a surface must satisfy the causality relation which is dictated by the wave equation. In other words, the seismic signals will not fill the whole time–space (or frequency–wavenumber) plane in arbitrary ways. There are a huge amount of points in the plane which actually do not satisfy the causality relation, and accordingly the seismic signals will not exist in these points. Take the case of homogeneous media as an example. The solution of the scalar wave equation

$$(-\partial_t^2 + \nabla^2)u(t, x) = 0 \quad (8)$$

only locates on the “light cone” in the time–space continuum [Fig. 1(a)] or in the frequency–wavenumber continuum [Fig. 1(b)]. For inhomogeneous media, this “light cone” can be roughly satisfied in each local area. It can be observed that the solution of the wave equation is actually very sparse in the whole volume, and the light cone is a critical constraint to

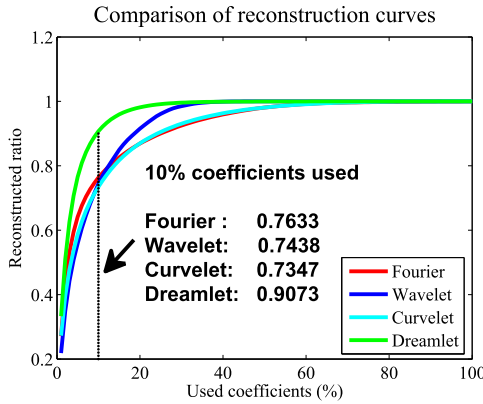


Fig. 2. Comparison of the representations of a seismic data set with different bases.

effectively represent wavefields [54]. That is one of the reasons why the dreamlet packet can have a better representation of seismic data compared with the mathematical atoms-based representations. The work presented in [55] gives the detailed derivation and proof.

Fig. 2 demonstrates a comparison of the representations of a seismic data set with different bases. Four kinds of basis, namely Fourier, Daubechies wavelet, curvelet, and dreamlet bases, are used to represent a field prestack data set with a high SNR. The abscissa denotes the number of the coefficients (in percentage) used for reconstruction, and the ordinate denotes the reconstructed ratio (RR), defined as

$$RR = \|\mathbf{U}'\|_F^2 / \|\mathbf{U}\|_F^2 \quad (9)$$

where \mathbf{U} is the original data and \mathbf{U}' is the reconstructed data. Symbol $\|\cdot\|_F$ denotes the Frobenius norm. It can be seen that the RR of dreamlet rises significantly faster than others, which indicates the superior performance of dreamlet for the sparse representation of seismic data.

C. Damped Dreamlet Representation for Signal Estimation

The dreamlet has a decent ability in the representation of the seismic data and thus can achieve an estimation of the true signal from the observed data. Consider an additive model [61]

$$\mathbf{U} = \mathbf{S} + \mathbf{N} \quad (10)$$

where \mathbf{U} is the observed seismic signal, \mathbf{S} is the true seismic signal, and \mathbf{N} represents the incoherent unwanted energies, including the random noise and irregularly missing data. With the help of dreamlet packet, we hold

$$\mathbf{U} = \mathbf{C}\mathbf{D} \quad (11)$$

where \mathbf{C} and \mathbf{D} are the coefficients and the dreamlet basis blocked in a row vector and a column vector, respectively. A typical assumption behind the dreamlet-based signal estimation problem is that the signal (\mathbf{S}) is compressible in the dreamlet domain but the noise (\mathbf{N}) is not. In other words, the energy of the signal is concentrated and compressed in the subspace spanned by several greater coefficients after the dreamlet transform (6) but the energy of noise disperses in the

whole space. Without loss of generality, we assume that the signal is k -sparse in the dreamlet domain, i.e., $\|\mathbf{SD}^{-1}\|_0 = k$. The signal estimation problem (estimate \mathbf{S} from \mathbf{U}) can be formulated as

$$\arg \min_{\mathbf{C}'} \|\mathbf{U} - \mathbf{C}'\mathbf{D}\|_F^2, \quad \text{s.t. } \|\mathbf{C}'\|_0 = k \quad (12)$$

where symbol $\|\cdot\|_0$ denotes the l_{zero} norm and k can be conceptually understood as analogous to the “bandwidth.” Equation (12) is actually used to find a signal-dimensional optimal approximation of the observed data under the least-squares constraint. Essentially, it is a least-squares projection of the high-dimensional vector (i.e., the observed data \mathbf{U}) on a signal-dimensional plane. This least-squares projection can be obtained by keeping the greater coefficients and setting others to zero, and the estimated signal can be obtained as [57], [58], [60]:

$$\mathbf{U}' = \mathbf{C}_k \mathbf{D}_k \quad (13)$$

where \mathbf{U}' denotes the estimated signal and \mathbf{C}_k and \mathbf{D}_k represents the k th greatest coefficients and the corresponding dreamlet basis. This strategy is also widely used in other sparse-promoting and low-rank-promoting transforms-based compressed sensing problem [31], [39], [52], [62], [63].

Equation (12) can obtain a satisfactory estimation of the true seismic signal indeed, because the dreamlet can represent the seismic data effectively. However, we have found that a more accurate estimation can be obtained by a damped version of (12). With the dreamlet basis, we can represent the signal \mathbf{S} and the noise \mathbf{N} as

$$\mathbf{S} = \mathbf{C}^S \mathbf{D} \quad (14)$$

$$\mathbf{N} = \mathbf{C}^N \mathbf{D} \quad (15)$$

where \mathbf{C}^S and \mathbf{C}^N denote the coefficients corresponding to \mathbf{S} and \mathbf{N} . As we assumed before, \mathbf{S} is highly sparse in the dreamlet domain but \mathbf{N} is not. That is to say that \mathbf{C}^S actually contains a huge number of zeros. Without loss of generality, we use \mathbf{C}_k^S to represent the nonzero coefficients and \mathbf{C}_{end-k}^S to represent the zero coefficients. So, we hold

$$\mathbf{S} = \mathbf{C}_k^S \mathbf{D}_k \quad (16)$$

and

$$\begin{aligned} \mathbf{C}_{end-k} \mathbf{D}_{end-k} &= (\mathbf{C}_{end-k}^S + \mathbf{C}_{end-k}^N) \mathbf{D}_{end-k} \\ &= \mathbf{C}_{end-k}^N \mathbf{D}_{end-k}. \end{aligned} \quad (17)$$

Combining (10) and (14)–(17), we hold

$$\mathbf{S} = (\mathbf{C}_k - \mathbf{C}_k^N) \mathbf{D}_k. \quad (18)$$

Equation (18) shows that \mathbf{S} can be represented as a damped version of (13). The only remaining problem is the value of \mathbf{C}_k^N . If \mathbf{N} is close to fully incompressible noise with the dreamlet basis (similar to the concept of white noise with the Fourier basis), it can be represented approximately as

$$\mathbf{N} \approx \sigma \mathbf{ID} \quad (19)$$

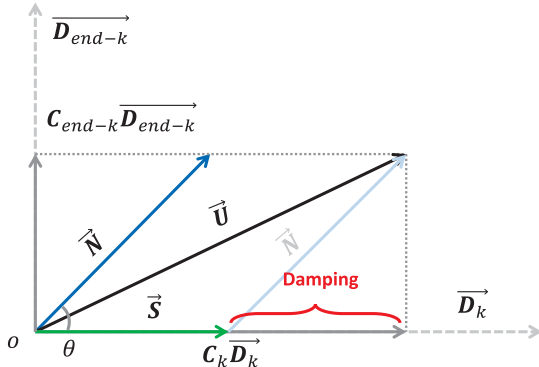


Fig. 3. Geometrical interpretation of the damped dreamlet representation.

where \mathbf{I} is the unit matrix and the constant σ denotes the energy level of noise. Therefore, the signal \mathbf{S} can be represented approximately as

$$\mathbf{S} \approx \bar{\mathbf{U}} = \mathbf{C}_k \mathbf{T} \mathbf{D}_k \quad (20)$$

$$\mathbf{T} = (\mathbf{I}_k - \text{diag}[|\sigma/c_j|]^\nu) \quad (21)$$

where $\bar{\mathbf{U}}$ is the estimated signal, \mathbf{T} is named as the damping operator, c_j , $j = 1 : k$ is the element of \mathbf{C} , $\text{diag}[\cdot]$ denotes the diagonal operator, and $\nu \geq 1$ is an introduced parameter, which can control the strength of the damping operator. The greater the ν value, the weaker the damping, and (20) reverts to (13) when $\nu \rightarrow \infty$. Although the “truncation” (i.e., the k) in the traditional dreamlet representation is chosen with broad range according to the data complexity, the choice of the damping factor ν is quite convenient. A smaller ν value (e.g., $\nu = 1$ or $\nu = 2$) will certainly improve the denoising strength but will have greater possibility at the cost of damaging useful signal. When the ν value is chosen as 3–5, or an even large value, the compromise between preservation of useful signals and removal of random noise is much improved. Therefore, taking the tradeoff between noise removal and signal preservation into consideration, the value of ν in the damped dreamlet representation can be generally chosen between 3 and 8 based on our experiments and experience. For the value of σ , one can use the average of the ($\text{end}-k$)th smallest elements of \mathbf{C} or more conveniently use c_{k+1} as an approximation.

D. Interpretation of Damped Dreamlet Representation

A geometrical interpretation of the proposed damped dreamlet representation is given in Fig. 3. The noise vector \vec{N} is between the dreamlet base vectors \vec{D}_k and $\vec{D}_{\text{end}-k}$ with an angle θ to \vec{D}_k because of the incompressibility of the noise. The angle θ relates to the position of k . The vector \vec{S} is on the base vectors \vec{A}_k , because \vec{S} can be completely represented by \vec{D}_k as we assumed before. Vector $\vec{U} = \vec{S} + \vec{N}$. From the principle of vector decomposition, \vec{U} can also be represented as $\mathbf{C}_k \vec{D}_k + \mathbf{C}_{\text{end}-k} \vec{D}_{\text{end}-k}$. The traditional dreamlet representation [57], [58], [60] uses $\mathbf{C}_k \vec{D}_k$ to approximate \vec{S} . It is effective, because we can obtain an estimation of \vec{S} in the signal-dimensional ($\mathbf{C}_k \vec{D}_k$ is actually a projection of \vec{U} onto

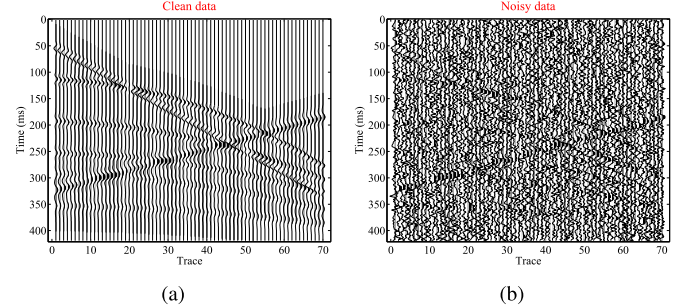


Fig. 4. Synthetic example. (a) Clean data. (b) Noisy data.

the signal-dimensional subspace spanned by \vec{D}_k). However, as we can see from Fig. 3, $\mathbf{C}_k \vec{D}_k \neq \vec{S}$, and the gap between $\mathbf{C}_k \vec{D}_k$ and \vec{S} (highlighted by the red brace) exactly equals to the projection of \vec{N} onto the subspace spanned by \vec{D}_k if we use the geometric knowledge. Thus, we hold

$$\vec{S} = \mathbf{C}_k \vec{D}_k - \mathbf{C}_k^N \vec{D}_k. \quad (22)$$

We can also observe that the projection of \vec{U} onto the subspace spanned by $\vec{D}_{\text{end}-k}$ exactly equals to the projection of \vec{N} onto this subspace. Thus, we hold

$$\mathbf{C}_{\text{end}-k}^N \vec{D}_{\text{end}-k} = \mathbf{C}_{\text{end}-k} \vec{D}_{\text{end}-k}. \quad (23)$$

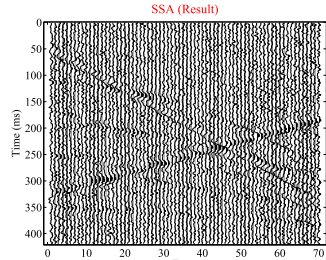
Even though \mathbf{C}_k^N is unknown, we can still obtain an estimation of \vec{S} under assumption (19), as shown in (20).

III. APPLICATION

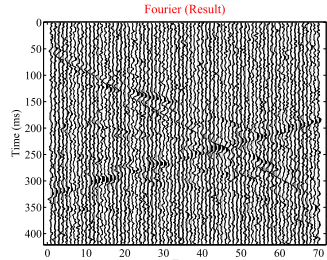
In this section, we apply the proposed damped dreamlet technique to solve two problems of seismic data processing, namely, the seismic random noise suppression and seismic data interpolation. We compare the proposed technique with the commonly used state-of-the-art mathematical atoms-based sparse representation and rank-reduction-based techniques using both synthetic and real examples.

A. Seismic Random Noise Suppression

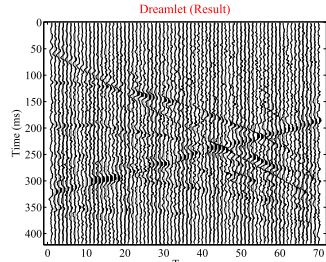
We first test the damped dreamlet technique on a synthetic example. The clean data are composed of five primaries and two linear events with crossover phenomenon, which are created by Ricker wavelets with different dominant frequencies, as shown in Fig. 4(a). The five primaries have an amplitude decrease gradually from top to bottom (from 1 to 0.6 with 0.1 interval). The purpose of this design (frequency and amplitude attenuating) is to make the synthetic model closer to the real case. We add band-limited (0–150 Hz) Gaussian noise to the clean data as shown in Fig. 4(b). The heavy noise contaminates the useful signals, the primaries, and the profile is extremely noisy. We use the rank-reduction, i.e., the SSA [11], the Fourier representation, the dreamlet representation, and the proposed damped dreamlet representation-based approaches to suppress the added noise, respectively. The denoised results are presented in Fig. 5. Fig. 6 shows the f-k spectra of the clean and noisy data and the four denoising results. Figs. 7 and 8



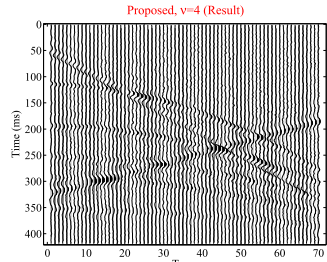
(a)



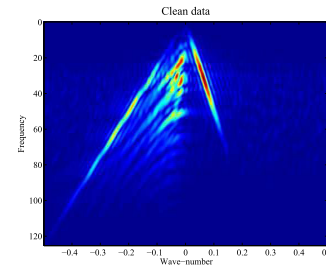
(b)



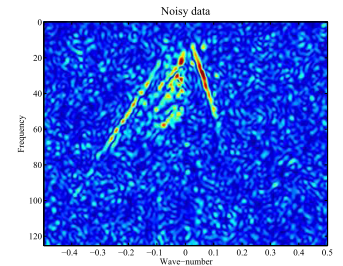
(c)



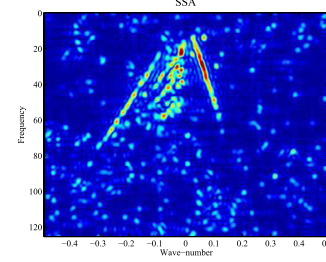
(d)



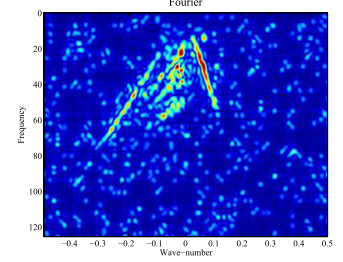
(a)



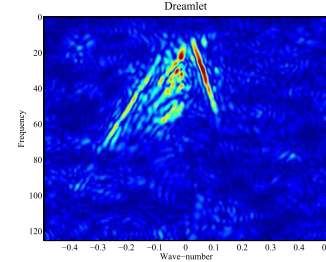
(b)



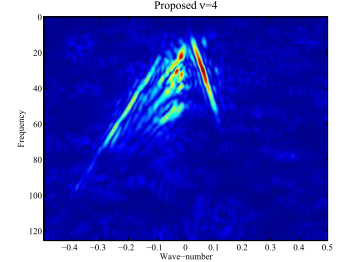
(c)



(d)



(e)



(f)

Fig. 5. Synthetic example. Denoised result using (a) rank-reduction approach, (b) Fourier representation-based approach, (c) dreamlet representation-based approach, and (d) damped dreamlet representation-based approach.

demonstrate the corresponding denoising error and remove noise sections. Here, the denoising error denotes the difference between true signal and denoised data and the removed noise section denotes the difference between noisy and denoised data. Table I lists the quantitative analysis of the denoising performance, in which two statistical indicators, namely SNR and cross correlation (CC), are used to evaluate the denoising performance. The definitions of S/N and CC are shown in the following:

$$\text{SNR} = 10 \log \frac{\|\mathbf{S}\|_F^2}{\|\mathbf{S} - \mathbf{U}\|_F^2} \quad (24)$$

$$\text{CC} = \frac{\sum \mathbf{S} \circ \mathbf{U}}{\sqrt{\|\mathbf{S}\|_F^2} \sqrt{\|\mathbf{U}\|_F^2}} \quad (25)$$

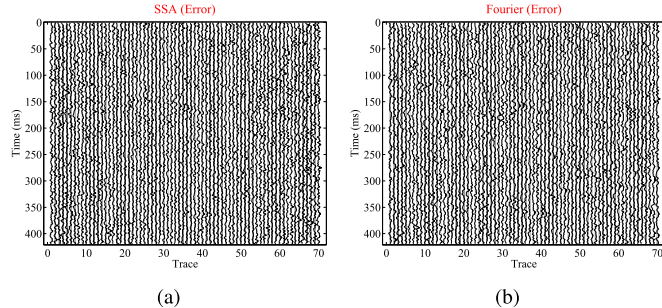
where \mathbf{S} denotes the clean data, and \mathbf{U} denotes the noisy data. The symbol \circ denotes the Hadamard product. A higher SNR or CC corresponds to a better denoising performance. In this example, we choose rank = 7 for the SSA approach and truncate the 90% smallest coefficients for both the Fourier and dreamlet representations. The damped dreamlet representation works with 90% smallest coefficients truncated and $v = 4$. As we can see from the synthetic example, it is clear that although all the approaches perform well and suppress the random noise, the proposed approach obtains even better results. To better test the performance of our method, we add random noise with different SNRs to the clean data and apply the four methods to the noisy data, respectively. Fig. 9 shows the SNR curves. We observe that the damped dreamlet representation method can always obtain a higher SNR compared with others.

To test the sensitivity of the proposed method on the parameter v , we try different v values and compare their performance. Fig. 10 shows the denoising performance of the

Fig. 6. Synthetic example. (a) and (b) f-k spectra of the clean and noisy data. (c)–(f) f-k spectra of the denoised results using the rank-reduction, Fourier representation, dreamlet representation, and proposed approaches.

synthetic data using different v values. Table II lists the corresponding quantitative analysis of the denoising performance. It is clear that as v value increases, the residual noise becomes stronger and stronger. When $v = 16$, the denoising performance gets closer to the traditional dreamlet representation, as shown in Fig. 10(d). However, when v is too small, say $v = 2$, although the denoised section [Fig. 10(a)] is very clean, there is some signal loss on the events. Therefore, a conservative choice of v will improve the compromise between preservation of useful signal and removal of random noise.

The next example explores the performance of the damped dreamlet-based method on field incoherent noise attenuation. The original profile is shown in Fig. 11. There is a significant amount of incoherent noise that corrupts the reflection signal. The size of data in this example is 1800×150 , with a sampling interval at 2 ms. Similarly, we use the four approaches to attenuate the incoherent noise and to compare their denoising performances. Fig. 12 shows the denoised results. Fig. 13 shows the f-k spectra of the clean and noisy data and the four denoising results. Fig. 14 shows the removed noise sections. For a detailed comparison, Fig 15 gives five magnified parts



(a)

(b)

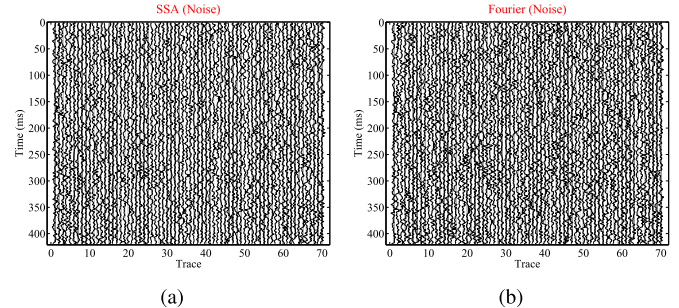
Dreamlet (Error)

Proposed, v=4 (Error)

(c)

(d)

Fig. 7. Synthetic example. Denoising error using (a) rank-reduction approach, (b) Fourier representation-based approach, (c) dreamlet representation-based approach, and (d) damped dreamlet representation-based approach.



(a)

(b)

(c)

(d)

Fig. 8. Synthetic example. Removed noise using (a) rank-reduction approach, (b) Fourier representation-based approach, (c) dreamlet representation-based approach, and (d) damped dreamlet representation-based approach.

TABLE I
QUANTITATIVE ANALYSIS OF THE DENOISING PERFORMANCE

	Input	SSA	Fourier	Dreamlet	Proposed
SNR	-15.7578	-5.8306	-6.0336	-1.8890	13.6601
CC	0.4089	0.5486	0.5358	0.6746	0.8788

from the raw data and four denoised data, as highlighted by the cyan frame boxes in Figs. 11 and 12. The truncations in this experiment are rank = 23 for the SSA approach and 90% for all the Fourier, dreamlet, and damped dreamlet representations. The damping factor v in the damped dreamlet representation is 3. As illustrated in Figs. 12–15, the damped dreamlet representation has the maximum incoherent noise reduction. The denoised seismic image using the proposed method is much cleaner than those using other methods.

B. Seismic Data Interpolation

The seismic data interpolation is implemented by an iterative damped dreamlet representation. Let \mathbf{O} represent the observation matrix which consists of 0 (representing observed grid points) and 1 (representing unobserved grid points), and \mathfrak{F} represents the damped dreamlet filtering (20). The iterative formula of \mathfrak{F} for seismic data interpolation can be written as

$$\bar{\mathbf{U}}^k = (1 - \lambda)\mathbf{U} + \lambda\mathfrak{F}\bar{\mathbf{U}}^{k-1} \circ (\mathbf{I} - \mathbf{O}) + \mathfrak{F}\bar{\mathbf{U}}^{k-1} \circ \mathbf{O} \quad (26)$$

where symbol \circ denotes the Hadamard product. k is the current iteration, \mathbf{I} denotes the matrix whose all elements are equal to 1, and $\lambda \in (0, 1]$ is the weight factor depending on the random noise level. The λ can be fixed or changed with the iteration. Similar iterative formula can also be found in [11], [57], and [58].

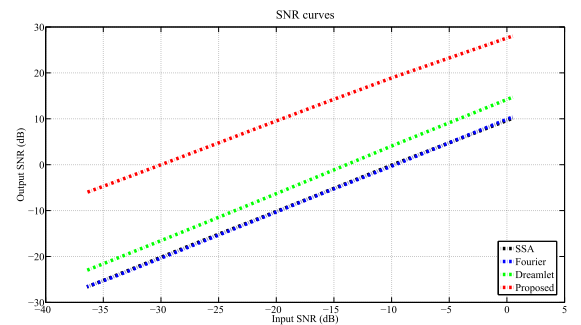


Fig. 9. Denoising comparison of the synthetic data with different SNRs using the rank-reduction, Fourier representation, dreamlet representation, and proposed approaches.

We first use a noise-free synthetic data set [the same as the example shown in Fig. 4(a)] to test the performance of signal interpolation of the damped dreamlet representation technique. The test data are shown again in Fig. 16(a). Fig. 16(b) shows the decimated data with approximately 40% of the traces irregularly removed from the original data [Fig. 16(a)]. The four approaches (i.e., the SSA, Fourier representation, dreamlet representation, and damped dreamlet representation) are used to recover the missing signals. Fig. 17 shows the reconstruction results and Fig. 18 shows the f-k spectra of the clean and decimated data and the four reconstruction results. Fig. 19 shows the reconstruction errors. Table III gives the quantitative comparison of the four approaches. We can observe that the SSA and Fourier representation work well when the events are flat but work poorly when the events are steep. We can see a lot of unrecovered signals from the error sections [Fig. 19(a) and (b)] as marked by the red arrows. The dreamlet representation has a satisfactory performance as we can see from

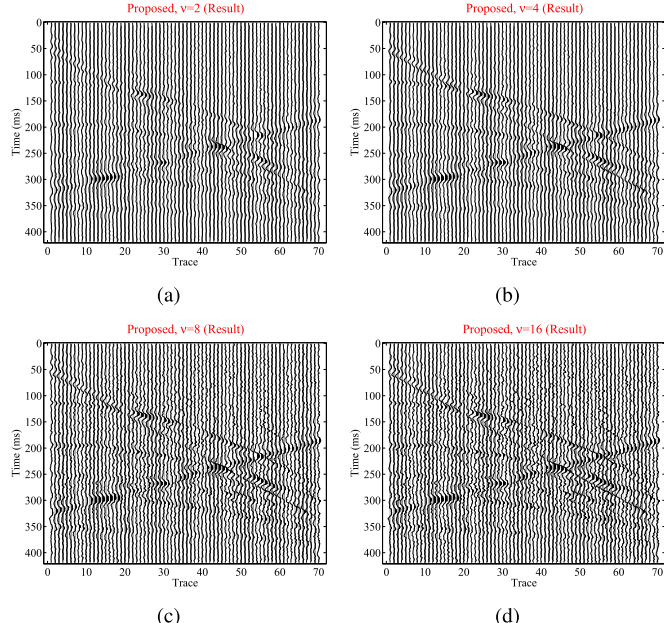


Fig. 10. Demonstration of the performance with different ν values. (a) $\nu = 2$.
 (b) $\nu = 4$. (c) $\nu = 8$. (d) $\nu = 16$.

TABLE II

QUANTITATIVE ANALYSIS OF THE DENOISING PERFORMANCE OF THE PROPOSED METHOD WITH DIFFERENT ν VALUES

	Input	$\nu = 2$	$\nu = 4$	$\nu = 8$	$\nu = 16$
SNR	-15.7578	10.3638	13.6601	2.7521	0.4310
CC	0.4089	0.8082	0.8788	0.7389	0.7084

Figs. 17(c) and 19(c) where almost all missing signals are recovered. However, the damped dreamlet representation performs better than the conventional dreamlet representation. From Table III, we can see that the damped dreamlet representation obtains the highest SNR and CC. The truncations in this experiment are rank = 7 for the SSA approach and 93% for all Fourier, dreamlet, and damped dreamlet representations. The damping factor ν in the damped dreamlet representation is 3. All the four approaches work with five iterations and $\lambda = 0$.

The next synthetic example is shown in Fig. 20. The clean data are the same as the previous examples as shown in Fig. 20(a). In order to test the antinoise performance of the proposed method for signal interpolation, we add band-limited (0–150 Hz) Gaussian noise to the clean data and then irregularly decimate approximately 40% of the traces. The decimated data are shown in Fig. 20(b). The interpolation results using the four approaches with ten iterations are presented in Fig. 21. Fig. 22 shows the f-k spectra of the clean and decimated data and the four interpolation results. The corresponding error sections are shown in Fig. 23. Table IV lists the quantitative comparison. The truncations in this experiment are rank = 7 for the SSA approach and 90% for all the Fourier, dreamlet, and damped dreamlet representations. The damping factor ν in the damped dreamlet representation is 3. λ in the iteration pattern (26) linearly increases with iteration from 0 to 1. All the four approaches work with ten iterations. Comparing

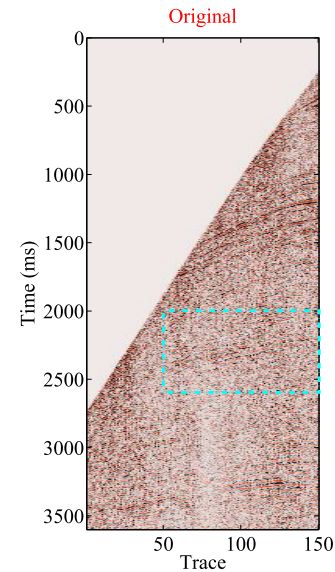


Fig. 11. Field example showing original data.

TABLE III
QUANTITATIVE ANALYSIS OF THE INTERPOLATION PERFORMANCE
OF THE FIRST SYNTHETIC EXAMPLE

	Input	SSA	Fourier	Dreamlet	Proposed
SNR	9.3938	21.8564	18.9131	27.1391	42.0483
CC	0.7805	0.9430	0.9221	0.9663	0.9925

TABLE IV
QUANTITATIVE ANALYSIS OF THE INTERPOLATION PERFORMANCE
OF THE SECOND SYNTHETIC EXAMPLE

	Input	SSA	Fourier	Dreamlet	Proposed
SNR	-6.3068	-0.6452	-4.5707	3.3199	14.5921
CC	0.3992	0.5811	0.4808	0.6727	0.9167

the results, we observe that the best result can be obtained with the damped dreamlet representation.

To demonstrate how the proposed approach works in practice, we apply the damped dreamlet representation on a real seismic data set. The original data set is shown in Fig. 24(a). This data set has 195 traces and 1200 time-samples per traces with a 2-ms time sampling interval. Again, we randomly remove approximately 40% of the traces, as shown in Fig. 24(b), and use the four methods to recover the signal. The interpolation results using the four methods are shown in Fig. 25. Fig. 26 shows the f-k spectra of the original and decimated data and the four interpolation results. Fig. 27 shows the difference between the data prior to decimation [Fig. 24(a)] and the result of interpolation (Fig. 25). The truncations in this experiment are rank = 10 for the SSA approach and 90% for all the Fourier, dreamlet, and damped dreamlet representations. The damping factor ν in the damped dreamlet representation is 4. λ in the iteration pattern (26) linearly increases with iteration from 0 to 1. As we can see from the result profiles, the SSA successfully recovers most missing signals. But the reconstructed section [Fig. 25(a)] is still noisy. The Fourier representation-based reconstruction gives an unsatisfying result [Fig. 25(b)], in which the decimated

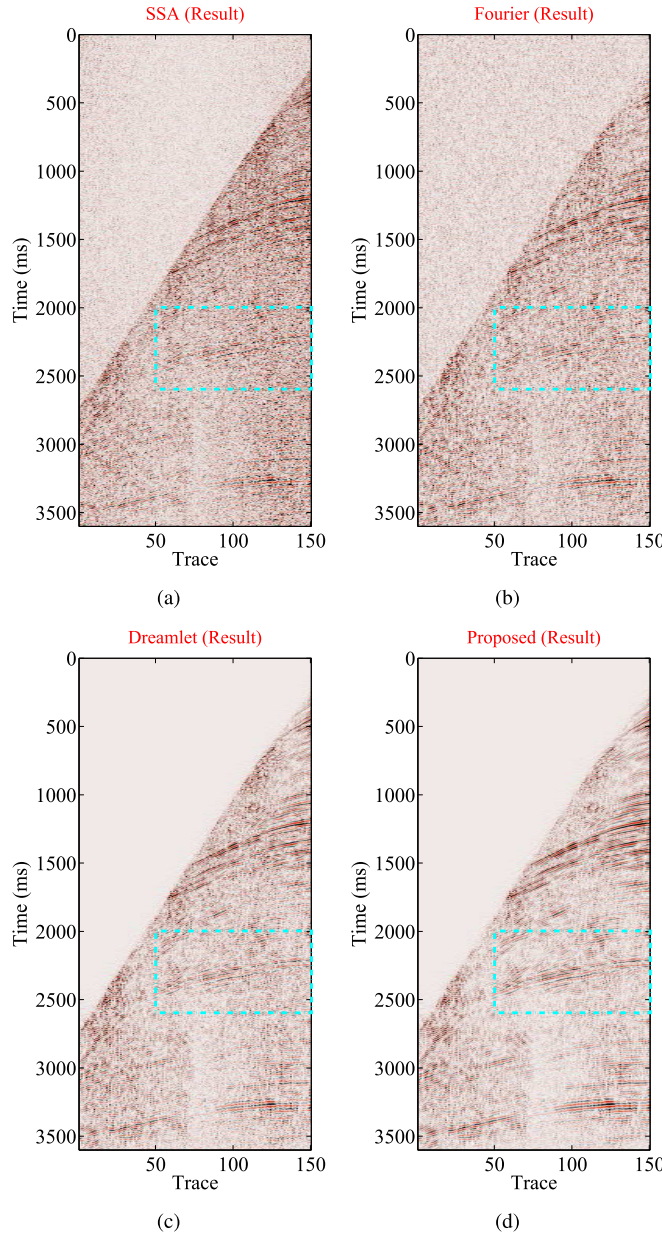


Fig. 12. Field example. Denoised result using (a) rank-reduction approach, (b) Fourier representation-based approach, (c) dreamlet representation-based approach, and (d) damped dreamlet representation-based approach.

signal and incoherent noise are notable. Both the traditional and damped dreamlet representation-based reconstructions work very well. The reconstructed sections [Fig. 25(c) and (d)] are smoother than before [Fig. 24(a)]. However, the damped dreamlet representation performs better than the traditional one, because we can observe unrecovered energies from both the interpolation [Fig. 25(c)] and difference [Fig. 27(c)] sections. The proposed damped dreamlet representation performs well in the case of an irregular decimation of the input data; however, it cannot interpolate regularly decimated data. For all the five examples, we do not use local processing windows to apply the four approaches. An interesting issue that can be found from this example is that the (damped) dreamlet representation-based approach will not introduce additional

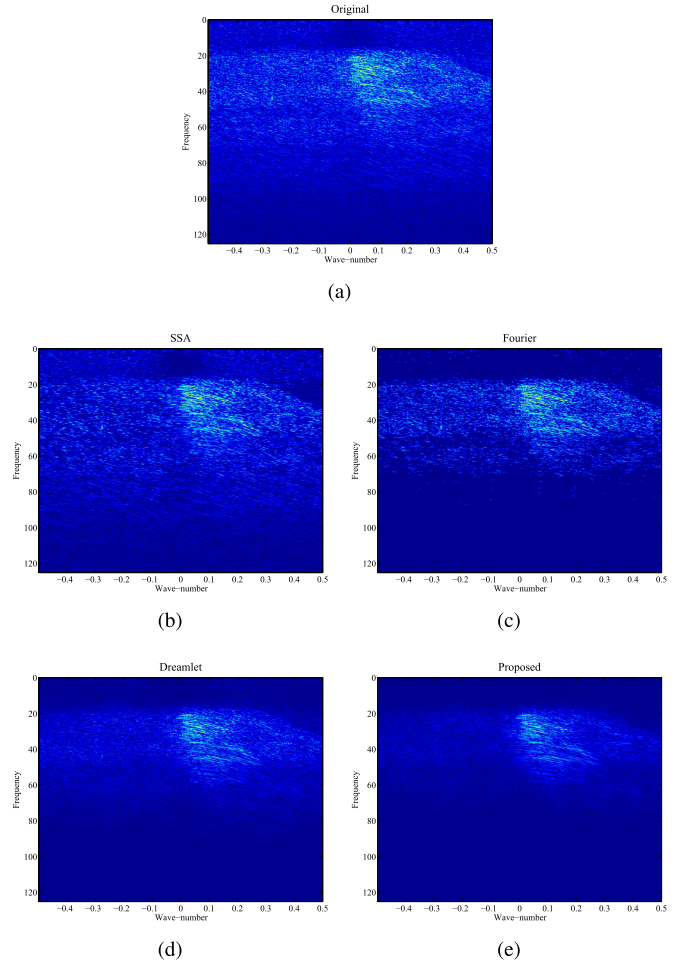


Fig. 13. Field example. (a) f-k spectrum of the original data. (b)–(e) f-k spectra of the denoised results using the rank-reduction, Fourier representation, dreamlet representation, and proposed approaches.

artificialities into the interpolation results, because the dreamlet atom (1) is a local atom. On the contrary, significant amounts of artificialities are introduced by the global SSA and Fourier representation, as we can see from the top-right parts of Fig. 25(a) and (b). This difference between the local and global techniques regarding the introduction of artificialities can also be observed from the previous example (Figs. 12 and 14).

IV. DISCUSSION

There are two important parameters in the presented approach that need to be chosen manually: the threshold and the damping factor. We rewrite the formula of signal estimation by the damped dreamlet representation as follows [(combine (20) and (21))]:

$$\mathbf{S} \approx \bar{\mathbf{U}} = \mathbf{C}_k (\mathbf{I}_k - \text{diag}[|\sigma/c_j|]^\nu) \mathbf{D}_k \quad (27)$$

where k is the threshold (truncation) and ν is the damping factor. It can be observed that k controls the number of the dreamlet basis (\mathbf{D}_k) which are used for the reconstruction of signal and ν controls the degree of damping the coefficients (\mathbf{C}_k) which corresponds to the kept dreamlet basis (\mathbf{D}_k). Both the two parameters determine the performance of

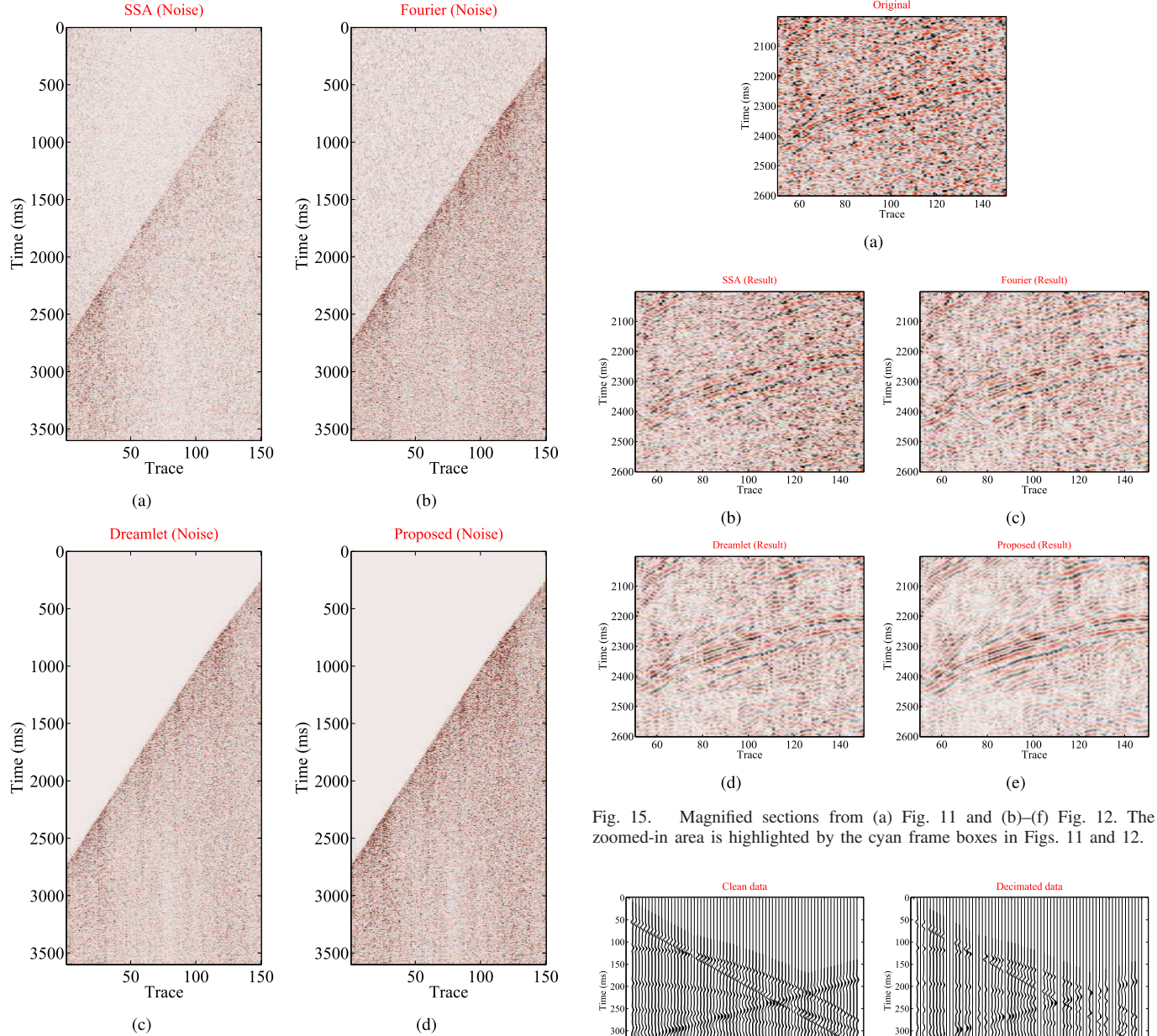


Fig. 14. Field example. Removed noise using (a) rank-reduction approach, (b) Fourier representation-based approach, (c) dreamlet representation-based approach, and (d) damped dreamlet representation-based approach.

the damped dreamlet representation approach. Like other sparse transform thresholding approaches (e.g., Fourier [47], wavelet [21], and curvelet [48] transforms), the choice of the threshold k is highly related to the complexity of the data (to be processed). When the data have a complex structure containing some factors, such as faults, thin layers, small-scale structures, diffraction points, and weak contrast interfaces, we may choose a great value for k (a mild truncation, e.g., truncating 80%, 75%, or 70% smallest coefficients) to preserve the weak reflection signal and the detailed information of subsurface structure. However, a great value for k will result in a poor performance of the damped dreamlet representation approach in attenuating random noise. When the data have a simple structure, we may choose a small value for k (a rigorous truncation, e.g., truncating 90% or 95% smallest

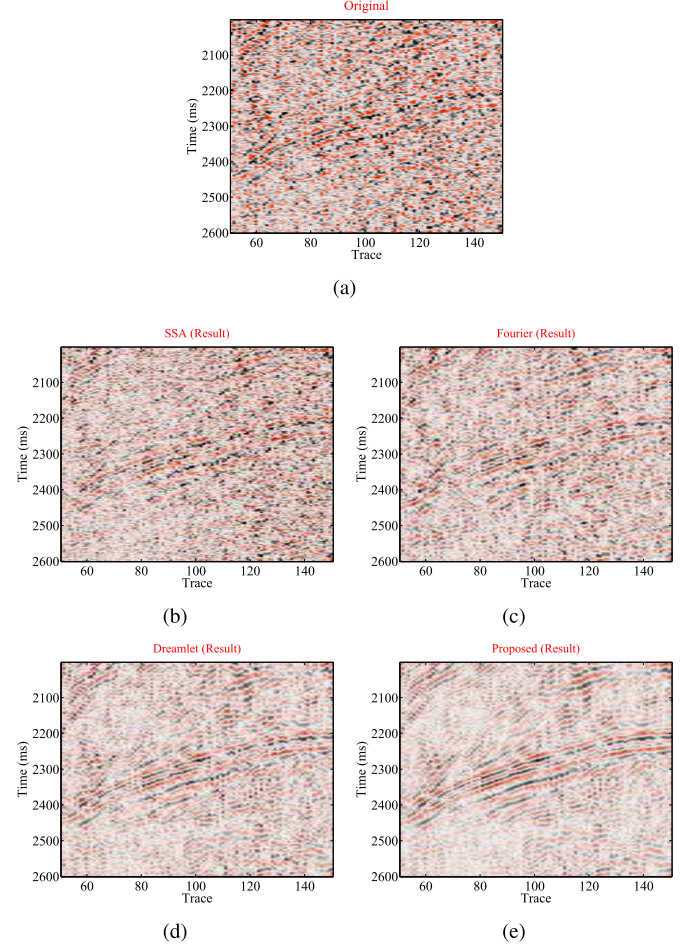


Fig. 15. Magnified sections from (a) Fig. 11 and (b)–(f) Fig. 12. The zoomed-in area is highlighted by the cyan frame boxes in Figs. 11 and 12.

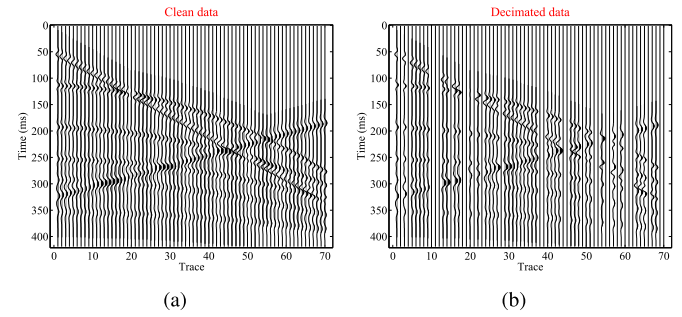


Fig. 16. First synthetic example. (a) Clean data. (b) Decimated data with approximately 40% of the traces missing.

coefficients) to obtain a strong denoising performance. The damping operator focuses on the suppression of residual noise in the subspace spanned by the kept dreamlet basis (\mathbf{D}_k). It acts on the coefficients (\mathbf{C}_k) to adjust linear combination of \mathbf{D}_k . The parameter ν is introduced to control the power of the damping operator. At present, we do not have an effective strategy to automatically choose a suitable damping factor ν in the application of the damped dreamlet representation approach. The parameters need to be tested before applying the proposed approach. Generally speaking, we test the threshold 5–7 times and the damping factor 2–3 times to find out the appropriate values. We should be careful to choose a small

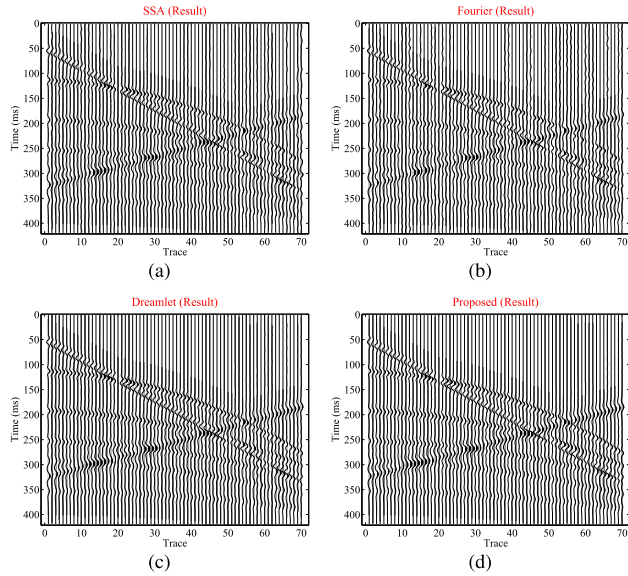


Fig. 17. First synthetic example. Interpolation result using (a) rank-reduction approach, (b) Fourier representation-based approach, (c) dreamlet representation-based approach, and (d) damped dreamlet representation-based approach.

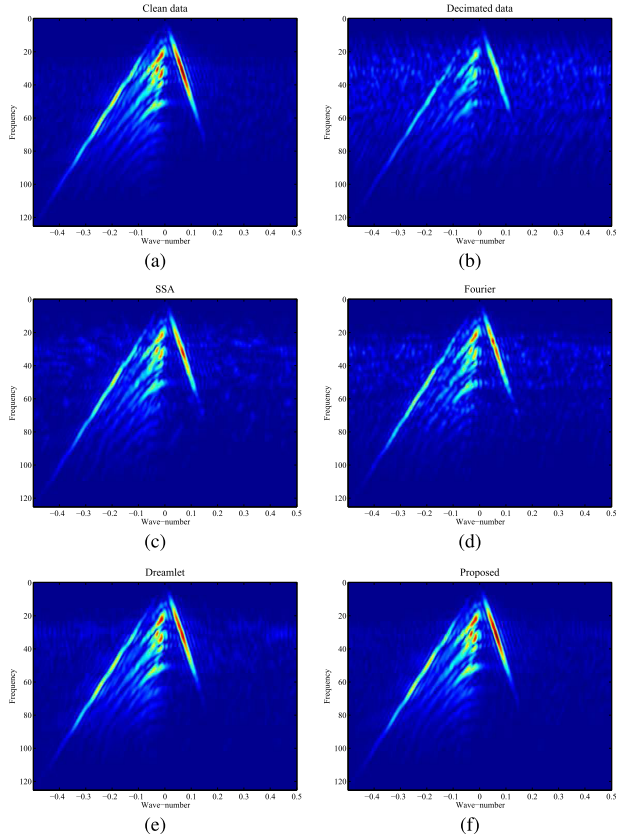


Fig. 18. First synthetic example. (a) and (b) f-k spectra of the clean and decimated data. (c)–(f) f-k spectra of the interpolation results using the rank-reduction, Fourier representation, dreamlet representation, and proposed approaches.

value for ν (e.g., 1 or 2), because it may cause overdamping of the coefficients C_k and further damage the signal.

Incorporating the damping operator will increase the computational cost of the dreamlet thresholding approach. Fig. 28 shows a comparison of computational costs of the traditional

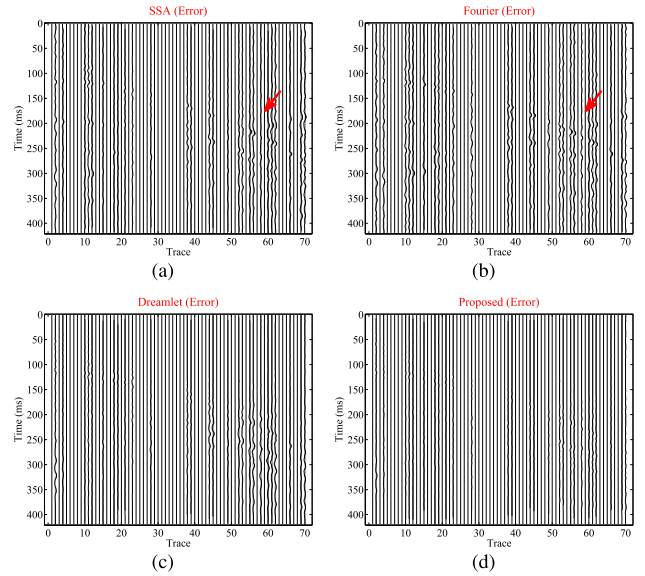


Fig. 19. First synthetic example. Interpolation error using (a) rank-reduction approach, (b) Fourier representation-based approach, (c) dreamlet representation-based approach, and (d) proposed approach.

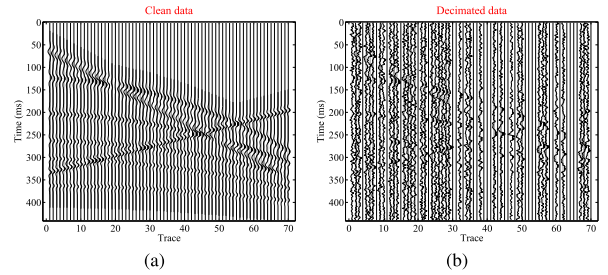


Fig. 20. Second synthetic example. (a) Clean data. (b) Decimated data with approximately 40% of the traces missing.

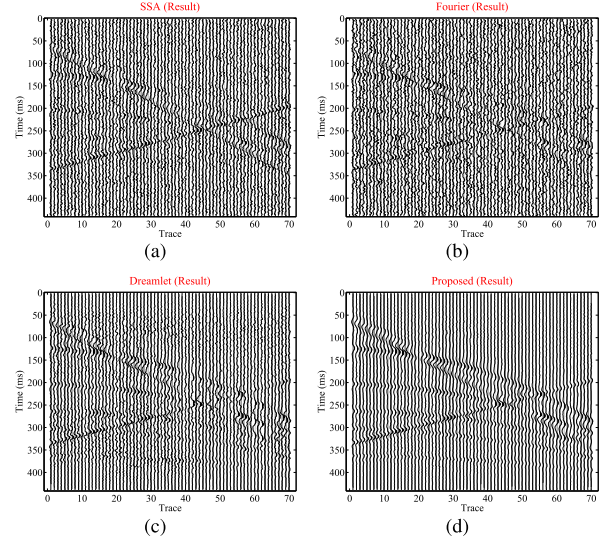


Fig. 21. Second synthetic example. Interpolation result using (a) rank-reduction approach, (b) Fourier representation-based approach, (c) dreamlet representation-based approach, and (d) proposed approach.

dreamlet representation and damped dreamlet representations with $\nu = 2$, $\nu = 4$, $\nu = 8$, and $\nu = 16$. The truncating ratio in the traditional and proposed dreamlet representation

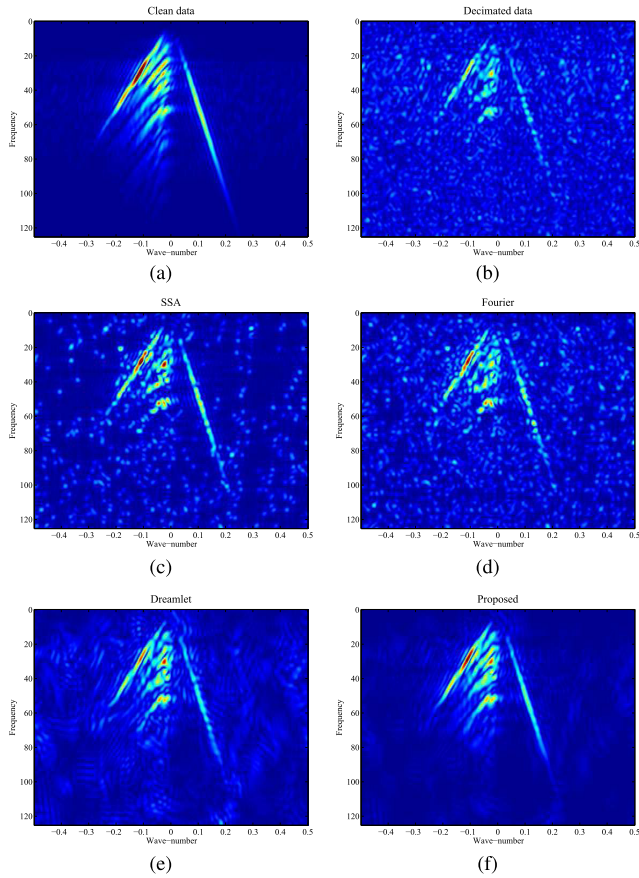


Fig. 22. Second synthetic example. (a) and (b) f-k spectra of the clean and decimated data. (c)–(f) f-k spectra of the interpolation results using the rank-reduction, Fourier representation, dreamlet representation, and proposed approaches.

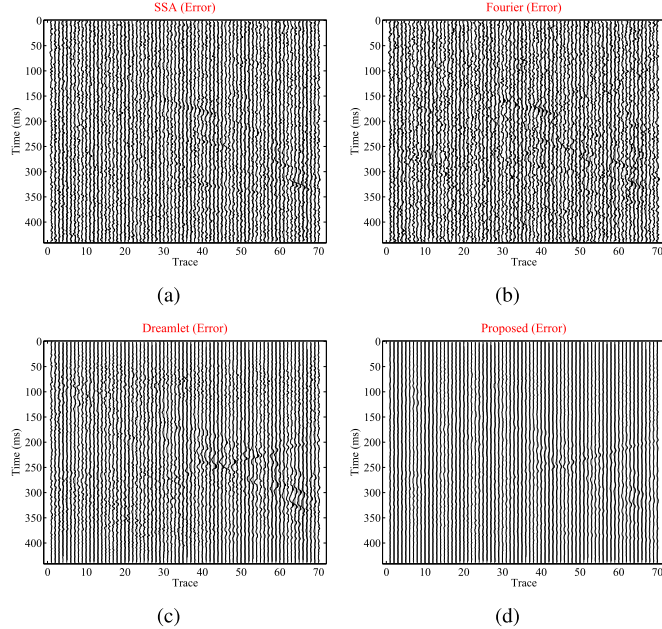


Fig. 23. Second synthetic example. Interpolation error using (a) rank-reduction approach, (b) Fourier representation-based approach, (c) dreamlet representation-based approach, and (d) damped dreamlet representation-based approach.

approaches varies from 50% to 95%. It can be observed that the truncation has a little influence on the computational cost of traditional dreamlet representation (red line).

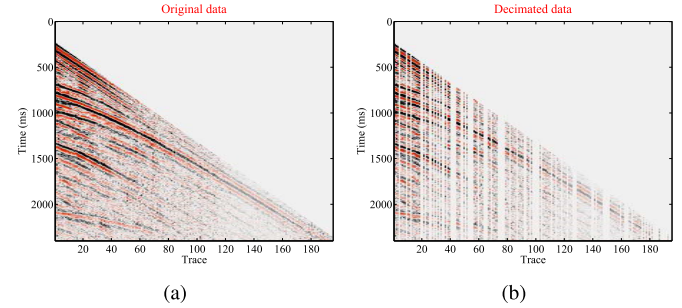


Fig. 24. Field example. (a) Original data. (b) Decimated data with approximately 40% of the traces missing.

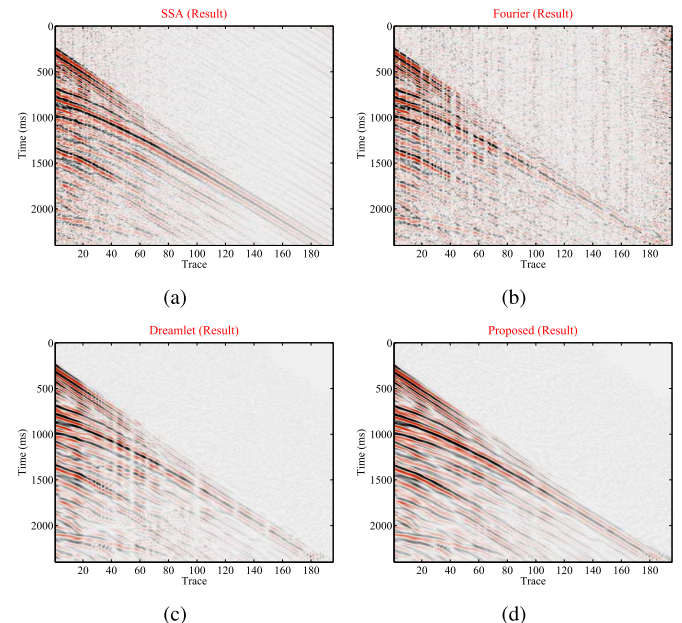


Fig. 25. Field example. Interpolation result using (a) rank-reduction approach, (b) Fourier representation-based approach, (c) dreamlet representation-based approach, and (d) damped dreamlet representation-based approach.

The computation time of damped dreamlet representation decreases as the truncating ratio increases. However, there is no significant difference among damped dreamlet representations with different ν values.

The proposed approach is effective for suppression of random noise but is limited for suppression of erratic noise [64], because the latter far from satisfies the assumption that the noise is incompressible in the dreamlet domain. The energy of erratic noise is mixed with that of useful signal in the dreamlet domain. Thus, it is difficult to separate them by dreamlet thresholding, especially in the case of strong erratic noise and weak signals. Recently, a number of researchers discussed incorporating a robust inversion framework to the sparse/lownrank representation to attenuate erratic noise. For example, the work in [64] proposed a robust parallel matrix factorization algorithm for erratic seismic noise attenuation, in which the traditional quadratic error criterion is replaced by a bisquare function, and the rank-reduction operator is implemented by the parallel matrix factorization algorithm. The work in [65]

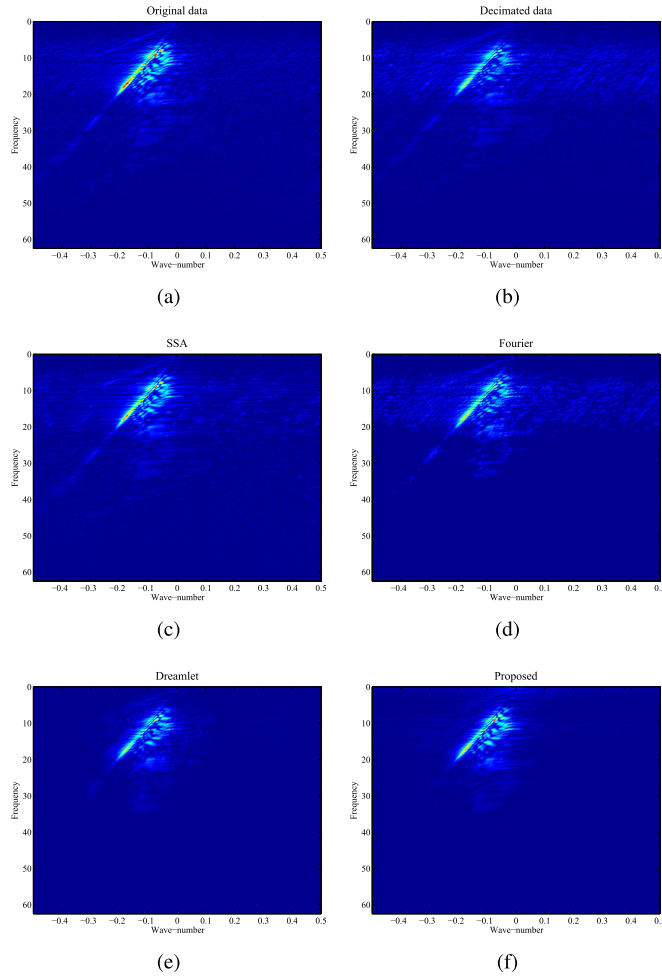


Fig. 26. Field example. (a) and (b) f-k spectra of the original and decimated data. (c)–(f) f-k spectra of the interpolation results using the rank-reduction, Fourier representation, dreamlet representation, and proposed approaches.

incorporated an l_1 misfit function to the Radon transform-based inversion problem to remove the erratic incoherent noise that arises in common receiver gather when simultaneous source data are acquired.

In the application section, we do not use local processing windows to apply the four approaches (i.e., the SSA, Fourier representation, dreamlet representation, and damped dreamlet representation-based approaches), because running the approaches without windowing can make us compare the approaches themselves and avoid the effect of windowing. In fact, taking local processing windows can help the data meet the sparse/low-rank assumptions required by the sparse/low-rank representation-based approaches. Because within a small data window, the structure of the data is relatively simple and the data will be sparse in the transform domain. However, when we implement the approach in local windows, the truncation (e.g., the percentage or rank) is even more difficult to choose, because the seismic data are highly nonstationary in both time and spatial dimensions, and the optimal truncation for different local windows is not consistent with each other. Several papers presented learning-based approaches, trying to represent data sparsely that do not need

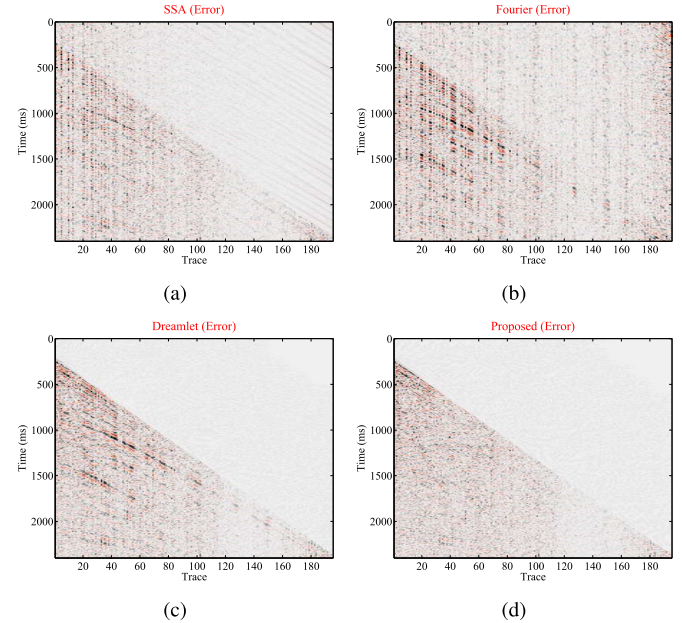


Fig. 27. Field example. Difference section using (a) rank-reduction approach, (b) Fourier representation-based approach, (c) dreamlet representation-based approach, and (d) damped dreamlet representation-based approach.

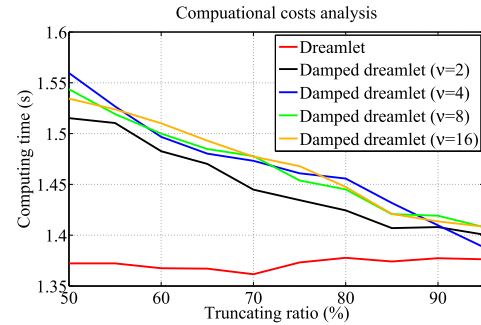


Fig. 28. Computational costs vary with the truncating ratio.

windowing [23]–[25], [66] or new transforms that can adapt to the windowed data [67].

V. CONCLUSION

We have proposed a novel technique of signal estimation from the noisy or incomplete seismic data based on dreamlet (drumbeat-beamlet) representation. As a type of physical wavelet, the dreamlet basis is more efficient to represent physical wavefield such as the seismic data compared with mathematical basis, such Fourier and curvelet. Moreover, a damping operator is derived and introduced into the process of dreamlet reconstruction which can significantly improve the performance of signal estimation of the dreamlet representation, because the damping operator can narrow the gap between the true signal and the dreamlet reconstruction. This new technique is named as the damped dreamlet representation. From the application of the damped dreamlet representation in seismic denoising and interpolation, it is obvious that the proposed method can obtain cleaner denoised image and recover signals better compared with the traditional

physical basis (dreamlet), mathematical basis (Fourier), and low-rank (SSA) representations. In the presented damped dreamlet representation approach, there are two important parameters that are chosen on the basis of experience and experiment: the threshold k (truncation) and the damping factor ν . It is foreseeable that the damped dreamlet representation can be beneficial not only in seismic wavefield processing but also in other physical wavefields, such as the electromagnetic wavefield, which make the proposed technique attractive to other research and promising for industrial applications.

REFERENCES

- [1] Y. Chen and S. Fomel, "Random noise attenuation using local signal-and-noise orthogonalization," *Geophysics*, vol. 80, no. 6, pp. WD1–WD9, 2015.
- [2] Y. Chen, Y. Zhou, W. Chen, S. Zu, W. Huang, and D. Zhang, "Empirical low-rank approximation for seismic noise attenuation," *IEEE Trans. Geosci. Remote Sens.*, vol. 55, no. 8, pp. 4696–4711, Aug. 2017.
- [3] G. Duncan and G. Beresford, "Median filter behaviour with seismic data," *Geophys. Prospecting*, vol. 43, no. 3, pp. 329–345, 1995.
- [4] L. L. Canales, "Random noise reduction," in *Proc. 54th Annu. Int. Meeting, SEG Tech. Program Extended Abstracts*, 1984, pp. 525–527.
- [5] B. M. Battista, C. Knapp, T. McGee, and V. Goebel, "Application of the empirical mode decomposition and Hilbert-Huang transform to seismic reflection data," *Geophysics*, vol. 72, no. 2, pp. H29–H37, 2007.
- [6] M. Bekara and M. van der Baan, "Random and coherent noise attenuation by empirical mode decomposition," *Geophysics*, vol. 74, no. 5, pp. V89–V98, 2009.
- [7] Y. Chen and J. Ma, "Random noise attenuation by $f - x$ empirical-mode decomposition predictive filtering," *Geophysics*, vol. 79, no. 3, pp. V81–V91, 2013.
- [8] N. Wu, Y. Li, and B. Yang, "Noise attenuation for 2-D seismic data by radial-trace time-frequency peak filtering," *IEEE Geosci. Remote Sens. Lett.*, vol. 8, no. 5, pp. 874–878, Sep. 2011.
- [9] Y. Liu, Y. Li, P. Nie, and Q. Zeng, "Spatiotemporal time-frequency peak filtering method for seismic random noise reduction," *IEEE Geosci. Remote Sens. Lett.*, vol. 10, no. 4, pp. 756–760, Jul. 2013.
- [10] Y. Tian and Y. Li, "Parabolic-trace time-frequency peak filtering for seismic random noise attenuation," *IEEE Geosci. Remote Sens. Lett.*, vol. 11, no. 1, pp. 158–162, Jan. 2014.
- [11] V. Orosez and M. Sacchi, "Simultaneous seismic data denoising and reconstruction via multichannel singular spectrum analysis," *Geophysics*, vol. 76, no. 3, pp. V25–V32, 2011.
- [12] S. Yuan and S. Wang, "A local $f - x$ Cadzow method for noise reduction of seismic data obtained in complex formations," *Petroleum Sci.*, vol. 8, no. 3, pp. 269–277, 2011.
- [13] W. Huang, R. Wang, Y. Chen, H. Li, and S. Gan, "Damped multi-channel singular spectrum analysis for 3D random noise attenuation," *Geophysics*, vol. 81, no. 4, pp. V261–V270, 2016.
- [14] M. A. N. Siahzar, S. Gholtashi, E. O. Torshizi, W. Chen, and Y. Chen, "Simultaneous denoising and interpolation of 3-D seismic data via damped data-driven optimal singular value shrinkage," *IEEE Geosci. Remote Sens. Lett.*, vol. 14, no. 7, pp. 1086–1090, Jul. 2017.
- [15] H. Li, R. Wang, S. Cao, Y. Chen, and W. Huang, "A method for low-frequency noise suppression based on mathematical morphology in microseismic monitoring," *Geophysics*, vol. 81, no. 3, pp. V159–V167, 2016.
- [16] W. Huang, R. Wang, Y. Zhou, and X. Chen, "Simultaneous coherent and random noise attenuation by morphological filtering with dual-directional structuring element," *IEEE Geosci. Remote Sens. Lett.*, vol. 14, no. 10, pp. 1720–1724, Oct. 2017.
- [17] W. Huang and R. Wang, "Random noise attenuation by planar mathematical morphological filtering," *Geophysics*, vol. 83, no. 1, pp. V11–V25, 2018.
- [18] G. Tang and J. Ma, "Application of total-variation-based curvelet shrinkage for three-dimensional seismic data denoising," *IEEE Geosci. Remote Sens. Lett.*, vol. 8, no. 1, pp. 103–107, Jan. 2010.
- [19] Y. Chen, S. Fomel, and J. Hu, "Iterative deblending of simultaneous-source seismic data using seislet-domain shaping regularization," *Geophysics*, vol. 79, no. 5, pp. V179–V189, 2014.
- [20] S. M. Mousavi, C. A. Langston, and S. P. Horton, "Automatic microseismic denoising and onset detection using the synchrosqueezed continuous wavelet transform," *Geophysics*, vol. 81, no. 4, pp. V341–V355, 2016.
- [21] R. Anvari, M. A. N. Siahzar, S. Gholtashi, A. R. Kahoo, and M. Mohammadi, "Seismic random noise attenuation using synchrosqueezed wavelet transform and low-rank signal matrix approximation," *IEEE Trans. Geosci. Remote Sens.*, vol. 55, no. 11, pp. 6574–6581, Nov. 2017.
- [22] S. M. Mousavi and C. A. Langston, "Automatic noise-removal/signal-removal based on general cross-validation thresholding in synchrosqueezed domain and its application on earthquake data," *Geophysics*, vol. 82, no. 4, pp. V211–V227, 2017.
- [23] S. Beckouche and J. Ma, "Simultaneous dictionary learning and denoising for seismic data," *Geophysics*, vol. 79, no. 3, pp. A27–A31, 2014.
- [24] Y. Chen, J. Ma, and S. Fomel, "Double-sparsity dictionary for seismic noise attenuation," *Geophysics*, vol. 81, no. 2, pp. V103–V116, 2016.
- [25] Y. Chen, "Fast dictionary learning for noise attenuation of multidimensional seismic data," *Geophys. J. Int.*, vol. 209, no. 1, pp. 21–31, 2017.
- [26] Y. Chen, S. Gan, T. Liu, J. Yuan, Y. Zhang, and Z. Jin, "Random noise attenuation by a selective hybrid approach using $f - x$ empirical mode decomposition," *J. Geophys. Eng.*, vol. 12, no. 1, pp. 12–25, 2015.
- [27] M. A. N. Siahzar, S. Gholtashi, A. R. Kahoo, H. Marvi, and A. Ahmadifar, "Sparse time-frequency representation for seismic noise reduction using low-rank and sparse decomposition," *Geophysics*, vol. 81, no. 2, pp. V117–V124, 2016.
- [28] M. A. N. Siahzar, S. Gholtashi, A. R. Kahoo, W. Chen, and Y. Chen, "Data-driven multitask sparse dictionary learning for noise attenuation of 3D seismic data," *Geophysics*, vol. 82, no. 6, pp. V385–V396, 2017.
- [29] S. Yuan, S. Wang, and G. Li, "Random noise reduction using Bayesian inversion," *J. Geophys. Eng.*, vol. 9, no. 1, p. 60, 2011.
- [30] S. Yuan and S. Wang, "Edge-preserving noise reduction based on Bayesian inversion with directional difference constraints," *J. Geophys. Eng.*, vol. 10, no. 2, p. 025001, 2013.
- [31] Y. Chen, "Iterative deblending with multiple constraints based on shaping regularization," *IEEE Geosci. Remote Sens. Lett.*, vol. 12, no. 11, pp. 2247–2251, Nov. 2015.
- [32] Y. Chen *et al.*, "Iterative deblending using shaping regularization with a combined PNMO-MF-FK coherency filter," *J. Appl. Geophys.*, vol. 122, pp. 18–27, Nov. 2015.
- [33] Y. Chen and Z. Jin, "Simultaneously removing noise and increasing resolution of seismic data using waveform shaping," *IEEE Geosci. Remote Sens. Lett.*, vol. 13, no. 1, pp. 102–104, Jan. 2016.
- [34] W. Huang, R. Wang, H. Li, and Y. Chen, "Unveiling the signals from extremely noisy microseismic data for high-resolution hydraulic fracturing monitoring," *Sci. Rep.*, vol. 7, no. 1, 2017, Art. no. 11996.
- [35] S. Yuan, S. Wang, M. Ma, Y. Ji, and L. Deng, "Sparse Bayesian learning-based time-variant deconvolution," *IEEE Trans. Geosci. Remote Sens.*, vol. 55, no. 11, pp. 6182–6194, Nov. 2017.
- [36] S. Spitz, "Seismic trace interpolation in the $f - x$ domain," *Geophysics*, vol. 56, no. 6, pp. 785–794, 1991.
- [37] M. J. Porsani, "Seismic trace interpolation using half-step prediction filters," *Geophysics*, vol. 64, no. 5, pp. 1461–1467, 1999.
- [38] M. Naghizadeh and M. D. Sacchi, "Multistep autoregressive reconstruction of seismic records," *Geophysics*, vol. 72, no. 6, pp. V111–V118, 2007.
- [39] J. Gao, J. Cheng, and M. D. Sacchi, "Five-dimensional seismic reconstruction using parallel square matrix factorization," *IEEE Trans. Geosci. Remote Sens.*, vol. 55, no. 4, pp. 2124–2135, Apr. 2017.
- [40] S. Trickett, "F-xy cadzow noise suppression," in *Proc. 78th Annu. Int. Meeting, SEG Techn. Program Extended Abstracts*, 2008, pp. 2586–2590.
- [41] Y. Chen, W. Huang, D. Zhang, and W. Chen, "An open-source Matlab code package for improved rank-reduction 3D seismic data denoising and reconstruction," *Comput. Geosci.*, vol. 95, pp. 59–66, Oct. 2016.
- [42] D. Zhang, Y. Chen, W. Huang, and S. Gan, "Multi-step damped multichannel singular spectrum analysis for simultaneous reconstruction and denoising of 3D seismic data," *J. Geophys. Eng.*, vol. 13, no. 5, p. 704, 2016.
- [43] Z. Wen, W. Yin, and Y. Zhang, "Solving a low-rank factorization model for matrix completion by a nonlinear successive over-relaxation algorithm," *Math. Programm. Comput.*, vol. 4, no. 4, pp. 333–361, 2012.
- [44] J. Gao, A. Stanton, and M. D. Sacchi, "Parallel matrix factorization algorithm and its application to 5D seismic reconstruction and denoising," *Geophysics*, vol. 80, no. 6, pp. V173–V187, 2015.
- [45] D. L. Donoho, "Compressed sensing," *IEEE Trans. Inf. Theory*, vol. 52, no. 4, pp. 1289–1306, Apr. 2006.
- [46] P. Zwartjes and A. Gisolf, "Fourier reconstruction with sparse inversion," *Geophys. Prospecting*, vol. 55, no. 2, pp. 199–221, 2007.

- [47] Y. Chen, K. Chen, P. Shi, and Y. Wang, "Irregular seismic data reconstruction using a percentile-half-thresholding algorithm," *J. Geophys. Eng.*, vol. 11, no. 6, p. 065001, 2014.
- [48] F. J. Herrmann and G. Hennenfent, "Non-parametric seismic data recovery with curvelet frames," *Geophys. J. Int.*, vol. 173, no. 1, pp. 233–248, 2008.
- [49] D. O. Trad, T. J. Ulrych, and M. D. Sacchi, "Accurate interpolation with high-resolution time-variant Radon transforms," *Geophysics*, vol. 67, no. 2, pp. 644–656, 2002.
- [50] A. Latif and W. A. Mousa, "An efficient undersampled high-resolution Radon transform for exploration seismic data processing," *IEEE Trans. Geosci. Remote Sens.*, vol. 55, no. 2, pp. 1010–1024, Feb. 2017.
- [51] S. Fomel and Y. Liu, "Seislet transform and seislet frame," *Geophysics*, vol. 75, no. 3, pp. V25–V38, 2010.
- [52] S. Gan, S. Wang, Y. Chen, X. Chen, W. Huang, and H. Chen, "Compressive sensing for seismic data reconstruction via fast projection onto convex sets based on seislet transform," *J. Appl. Geophys.*, vol. 130, pp. 194–208, Jul. 2016.
- [53] G. Kaiser, *A Friendly Guide to Wavelets*. Berlin, Germany: Springer, 1994.
- [54] D. Mu *et al.*, *Seismic Imaging, Fault Damage and Heal*. Berlin, Germany: Walter de Gruyter, 2014.
- [55] R.-S. Wu, Y. Geng, and B. Wu, "Physical wavelet defined on an observation plane and the dreamlet," in *Proc. 81th Annu. Int. Meeting, SEG Tech. Program Extended Abstracts*, 2011, pp. 3835–3839.
- [56] R.-S. Wu, Y. Wang, and M. Luo, "Beamlet migration using local cosine basis," *Geophysics*, vol. 73, no. 5, pp. S207–S217, 2008.
- [57] B. Wang, R.-S. Wu, Y. Geng, and X. Chen, "Dreamlet-based interpolation using POCS method," *J. Appl. Geophys.*, vol. 109, pp. 256–265, Oct. 2014.
- [58] B. Wang, R.-S. Wu, X. Chen, and J. Li, "Simultaneous seismic data interpolation and denoising with a new adaptive method based on dreamlet transform," *Geophys. J. Int.*, vol. 201, no. 2, pp. 1182–1194, 2015.
- [59] W. Huang, R. Wang, X. Chen, and Y. Chen, "Double least-squares projections method for signal estimation," *IEEE Trans. Geosci. Remote Sens.*, vol. 55, no. 7, pp. 4111–4129, Jul. 2017.
- [60] R.-S. Wu, Y. Geng, and L. Ye, "Preliminary study on Dreamlet based compressive sensing data recovery," in *Proc. 83th Annu. Int. Meeting, SEG Tech. Program Extended Abstracts*, 2013, pp. 3585–3590.
- [61] W. Huang, R. Wang, Y. Yuan, S. Gan, and Y. Chen, "Signal extraction using randomized-order multichannel singular spectrum analysis," *Geophysics*, vol. 82, no. 2, pp. V69–V84, 2016.
- [62] Y. Zhou, J. Gao, W. Chen, and P. Frossard, "Seismic simultaneous source separation via patchwise sparse representation," *IEEE Trans. Geosci. Remote Sens.*, vol. 54, no. 9, pp. 5271–5284, Sep. 2016.
- [63] Y. Chen *et al.*, "Simultaneous denoising and reconstruction of 5-D seismic data via damped rank-reduction method," *Geophys. J. Int.*, vol. 206, no. 3, pp. 1695–1717, 2016.
- [64] K. Chen and M. D. Sacchi, "Robust reduced-rank seismic denoising," in *Proc. SEG Tech. Program Expanded Abstracts*, 2013, pp. 4272–4277.
- [65] A. Ibrahim and M. D. Sacchi, "Simultaneous source separation using a robust Radon transform," *Geophysics*, vol. 79, no. 1, pp. V1–V11, 2014.
- [66] A. Ibrahim, P. Terenghi, and M. Sacchi, "Interpolation in presence of diffracted energy via a Stolt dictionary with sparsity constraints," in *Proc. 78th EAGE Conf. Exhibit.*, 2016, pp. 1–5.
- [67] A. Ibrahim, P. Terenghi, and M. D. Sacchi, "Wavefield reconstruction using a Stolt-based asymptote and apex shifted hyperbolic Radon transform," in *Proc. Int. Meeting, SEG Tech. Program Expanded Abstracts*, 2015.



Weilin Huang received the B.S. degree in mathematics and applied mathematics and the M.S. degree in computational mathematics from the China University of Petroleum, Beijing, China, in 2012 and 2015, respectively, where he is currently pursuing the Ph.D. degree in geophysics.

In 2016, he was a Visiting Ph.D. Student with the University of California at Santa Cruz, Santa Cruz, CA, USA. His research interests include seismic signal processing, microseismic monitoring, and seismic inversion.



Ru-Shan Wu received the B.Sc. degree in physics from Northwestern University, Xi'an, China, in 1962, and the Ph.D. degree in geophysics from the Massachusetts Institute of Technology (MIT), Cambridge, MA, USA, in 1984.

He was a Visiting Scientist at MIT from 1978 to 1981. He was a Research Scientist at MIT from 1984 to 1985, where he did his post-doctoral research. He was with the Institute of Geophysical Prospecting, Ministry of Geology, Beijing, China, from 1962 to 1978, and the Institute of Geophysics, Chinese Academy of Sciences, Beijing, from 1988 to 1990. In 1986, he moved to the University of California at Santa Cruz, Santa Cruz, CA, USA, where he is currently a Research Geophysicist and the Director of the Modeling and Imaging Laboratory, Institute of Geophysics and Planetary Physics. His research interests include seismic wave propagation and imaging in heterogeneous media, prestack depth migration, fast methods for elastic wave modeling, scattering and attenuation, holography, diffraction and scattering tomography, and general inversion of wavefields.



Runqiu Wang received the Ph.D. degree in geophysics from the China University of Petroleum, Beijing, China, in 2004.

He is currently a Professor with the China University of Petroleum. His research interests include the basic theory of geophysical exploration, seismic data processing, and microseismic monitoring.